ORNL/Sub--85-21674/1

DE87 011976

ORNL/Sub/85-21674/1
Dist. Category UC-11, 70

PERMEABILITY OF SHALE AT ELEVATED TEMPERATURE AND PRESSURE: TEST METHODOLOGY AND PRELIMINARY RESULTS

by

L.R. Myer and T.L. Christian

Date of Issue -- May 1987

Prepared at
Lawrence Berkeley laboratory
One Cyclotron Road
Berkeley, California 94720
under
Subcontract No. 10X-21674V

for

OAK RIDGE NATIONAL LABORATORY
Oak Ridge, Tennessee 37831
operated by
MARTIN MARIETTA ENERGY SYSTEMS, INC.
for the
U.S. DEPARTMENT OF ENERGY
under Contract No. DE-AC05-840R21400

Table of Contents

List of Figures

Introduction

Siting, design, and construction of a high-level radioactive waste repository will require predictive modelling of the groundwater flow in the rock mass in which the repository is located. One of the most important parameters in these models is the rock mass permeability, or hydraulic conductivity, a parameter which must be known for stress and temperature conditions representative of *in situ* conditions likely to exist in and around a repository. In general, fluid will flow through both the fractures and the rock matrix material between the fractures. The relative permeability of these two components influences to a great extent the type of hydrologic model to be used.

The Sedimentary Rock Program (SERP) at Oak Ridge National Laboratory (ORNL) has evaluated a variety of sedimentary rocks as potential host lithologies for a repository; shale was determined to be the rock type with the greatest potential (Croff *et al.*, 1987). This report represents the initial effort to characterize the permeability of selected shales, which are the focus of varied mineralogical, chemical and physical studies by SERP.

Studies of shale as a potential media for siting of a repository have been limited by the lack of hydrologic data, particularly under relevant *in situ* conditions. A laboratory test program was therefore initiated with the objectives of: 1) obtaining measurements of rock matrix and fracture permeabilities for different shales, and 2) evaluating the effect of temperature and pressure on these properties. The rock-matrix measurements will be discussed in this report.

One difficulty in attempting to determine representative hydrologic properties of shale is that there is a very wide range of rock types which are loosely classified as 'shale.' For this study 'end members' of a shale classification scheme developed by ORNL were selected for permeability measurements. The end members represent compositional extremes. The rocks studied were the Green River Formation, the Pierre Shale, and a Devonian

shale. To date testing has been conducted only on Green River samples. Pierre Shale and Devonian shale samples will be tested and results reported at a later date. A fourth 'end member,' the Lower Paleozoic Shale, has not been included because samples of sufficient size and physical integrity are not yet available.

This report presents the theory and methodology for measuring the hydraulic conductivity of very low permeability rocks such as shale. The test apparatus is described and problems associated with practical application of the theory are discussed. Results of hydraulic conductivity measurements on Green River Formation samples at 10 MPa effective pressure over the temperature range of 25 ° C to 140 ° C are discussed.

Theory

Available information (Young 1964, Brace 1980, Neuzil *et al.*, 1981) indicates shale matrix permeability data to be in the submicrodarcy (10^{-18} m^2) range. For permeability measurements in this range it is impractical to use standard steady-state methods. Brace *et al.* [1968] developed a technique based on the transient decay of a pressure pulse applied to a sample (now referred to either as pulse decay or transient pulse method). In this method, presented schematically in Figure 1, a sample and two fluid volumes, 'upstream and downstream reservoirs,' are brought to an equilibrium pore pressure (Pp). An instantaneous pressure pulse (PP) is then imposed on one end of the sample bringing the pressure at that end to Pp + PP. The subsequent decay of PP as a function of time can be related to sample hydraulic conductivity.

In particular, assuming validity of Darcy's law, the equation for one-dimensional transient flow of a compressible fluid through a porous compressible medium is given by:

$$\frac{\delta^2 P}{\delta x^2} = \frac{S_s}{K} \frac{\delta P}{\delta t} \qquad [1]$$

where

P = pressure head (L)

S_s = specific storage of the sample (L^{-1})

K = $k \gamma_w / \mu$ is the hydraulic conductivity of the sample(L/T); μ is viscosity of the fluid (M/LT); k is permeability (L^2); γ_w is specific weight of the fluid ($M/T^2L^{2)}$.

t = time (T)

x = distance along sample (L)

For an experimental configuration, such as shown conceptually in Figure 1, Hsieh *et al.* [1981] solved equation [1] for the boundary condition of an instantaneous increase in pressure of magnitude PP in the upstream reservoir. Using the general solution, Hsieh *et al.* [1981] examined two limiting cases of interest. In the first case, it was assumed that the sample specific storage was much less than the compressive storage of the upstream reservoir. In this case, the expression for dimensionless pressure in the upstream reservoir is:

$$P_u/PP = \frac{1}{1+\gamma} + \frac{\gamma}{1+\gamma} \exp\left[\frac{KAt}{S_u l}\left[-\frac{(1+\gamma)}{\gamma}\right]\right] \qquad [2]$$

and for dimensionless pressure in the downstream reservoir is:

$$P_d/PP = \frac{1}{1+\gamma} - \frac{1}{1+\gamma} \exp\left[\frac{KAt}{S_u l}\left[-\frac{(1+\gamma)}{\gamma}\right]\right] \qquad [3]$$

where A is the cross-sectional area of the sample, l is the length of the sample and $\gamma = S_d/S_u$, the ratio between compressive storage of the downstream (S_d) and upstream (S_u) reservoirs; compressive storage is defined as the change in volume of the reservoir per unit change in pressure head in the reservoir. This case is equivalent to the solution derived by Brace *et al.* [1968]. The second limiting case, that of large dimensionless time, yields expressions similar in form to equations [2] and [3] because at large times the effect of specific storage, S_s, becomes negligible (Hsieh *et al.*, 1981).

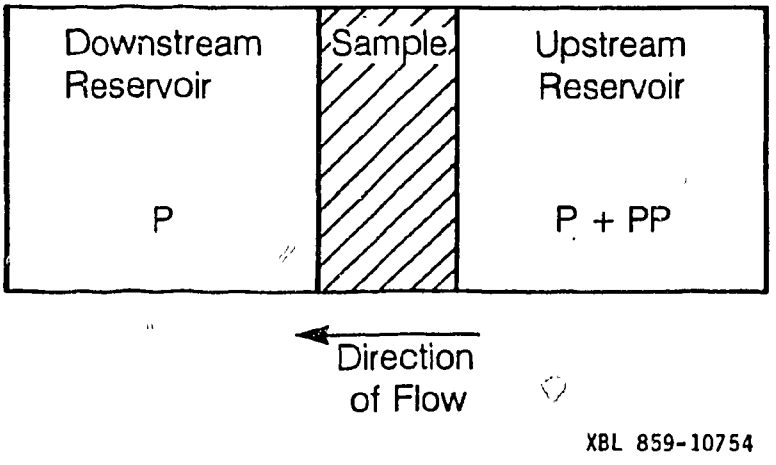

Figure 1. Conceptual illustration of pulse decay permeability test method (after Hsieh *et al.* 1981).

In practice, changes in differential pressure, ΔP, between the two reservoirs are measured as a function of time. Taking the difference between equation [2] and [3] yields:

$$\Delta P/PP = \exp\left[-\frac{KAt}{l}\left(\frac{1}{S_d}+\frac{1}{S_u}\right)\right] \qquad [4]$$

From this expression it is seen that the hydraulic conductivity can be obtained from the slope of a semi-log plot of the dimensionless differential pressure versus time. S_d and S_u, the compressive storage of the reservoirs, are specific parameters of the test apparatus and are measured independently.

Previous Measurements

Using the theory described above, numerous studies have been carried out to investigate the effects of stress on the permeability of low permeability rocks. Brace *et al.* [1968] found that the permeability of Westerly Granite decreases nonlinearly from about 1.55 x 10^{-17} m^2 at 9MPa effective pressure (confining presure minus pore pressure, P_c -P_p), to about 4.2 x 10^{-21} m^2 at 409.5 MPa effective stress. Kranz *et al.* [1979] observed a linear relation between effective pressure and the log of permeability for Barre Granite. Trimmer *et al.* [1980] observed the same relationship for effective pressures of 10MPa to 30Mpa for Westerly Granite, but for a gabbro, permeability (1 x 20^{-22} m^2 - 1 x 10^{-23} m^2) was nearly linear with effective pressure. In fitting experimental results on Chelmsford and Barre Granite, Bernabe [1986] assumed that permeability raised to a fractional power was proportional to the logarithm of confining pressure. Jones [1975] and Jones and Owens [1980] observed that increasing confining pressure reduced permeability in carbonate rocks and in gas sands, and found that the cube root of permeability was a linear function of the logarithm of confining pressure. These observations of decreasing permeability with effective hydrostatic pressure have generally

been attributed to microcrack closure under increasing pressure (Walsh and Brace 1984, Bernabe 1987).

Investigating the effects of differential stress level on permeability, Zoback and Byerlee [1975] observed an initial 30% decrease in permeability of Westerly Granite when a differential stress of about 50% of the rock strength was applied and a 3 fold increase of permeability at 39MPa effective pressure and differential stress approaching 90% of the rock strength. Trimmer *et al.* [1980] observed similar phenomena in Creighton Gabbro but with an increase of permeability of 7 fold when 88% of fracture stress had been reached at an effective stress of 25 MPa. These investigators concluded that the increase in permeability with differential stress reflects microcrack dilatancy which occurs when rock approaches failure.

Investigating hysteresis in permeability measurements during load cycling and the effective stress law, Kranz *et al.* [1979] observed that the permeability of Barre Granite depended upon the order of application of confining pressure and pore pressure. At the same effective stress state, permeability was higher for the case in which pore pressure was lowered to reach the desired effective stress state than for the case in which pore pressure was increased to reach the same state. Bernabe [1986] also found a path dependent permeability for Barre Granite (though not for Chelmsford Granite) and hysteresis and stress history effects under hydrostatic pressure. In addition he observed that these effects diminished as the number of loading cycles increased. Hysteresis and path dependent effects on permeability have been attributed to loading induced frictional sliding along grain boundaries and cracks, which, upon unloading is not recovered (Bernabe 1987).

The effects of stress on microcrack deformation and hence permeability, as discussed above, imply that the assumptions of constant specific storage and permeability in equation [1] are not strictly valid for cases involving large changes in effective stress. In particular, errors may be introduced in

determining permeability from tests in which the ratio between the applied pressure pulse and the pore pressure is large. However, the magnitude of this error has not been clearly established. Waldur and Nur [1986] found a 50% difference in the permeability of the Spirit River Sandstone for a pressure pulse magnitude of 40% of the pore pressure. On the other hand, Reda and Hadley [1986] found only a 14% difference in permeability of fractured welded tuff between steady-state and transient measurements with pressure pulses in excess of 100% of pore pressure. It is common practice in transient measurements to use a pressure pulse magnitude equal to 10% or less of the pore pressure.

Very few tests on low permeability rocks have been performed to study the effects of temperature on permeability. Using steady state methods Summers *et al.* [1978] observed that initial room temperature permeability of Westerly Granite increased by 1 to 2 orders of magnitude when heated to temperatures of 100 to 400 ° C. These investigators also observed that this permeability was time dependent in that after 1/2 day of flow the permeability decreased, approaching the original room temperature permeability or lower. They attributed the increase in permeability to differential thermal expansion of the minerals and the reduction due to dissolution of the minerals. From measurements of porosity changes in Westerly Granite as a function of temperature up to 300 ° C, Heard and Page [1982] inferred a three-fold increase in permeability at 7.6 MPa confinement but only about a 25% increase at 55 MPa confining pressure. Similarly, Heard [1980] inferred a 5 fold increase in permeability under no confinement compared to a 2 fold increase under 27.6 MPa confining pressure in Climax Quartz Monzonite. Heard attributed this increase in permeability to the effects of thermal expansion on the microcrack porosity of the material.

There are very few available data on the permeability of shales. Young [1964], using a modified steady state flow method, determined matrix permeabilities of coarse siltstones (5%-15% clay) to vary from 1.5 x 10^{-20} m^2 to

2.4 x 10^{-22} m^2 depending upon effective stress. Young hypothesized that as clay content increased permeability decreased. Pandy *et al.* [1974] inferred permeability of shales from gas diffusion measurements to be on the order of 10^{-15} m^2. Brace [1980] quoted shale permeabilities from various sources to range from 10^{-18} m^2 to 10^{-23} m^2. In particular, he reported *in situ* measurements of Pierre Shale permeability in the range of 10^{-18} to 10^{-19} m^2. Neuzil *et al.* [1981] measured the hydraulic conductivity of samples of Pierre and Wellington Formations, finding values of 1.9 x 10^{-12} m/sec and 5.2 x 10^{-18} m/sec, respectively. Mitchell [1976] reported the permeabilities of unconsolidated clays to be in the range of 10^{-17} m^2 to 10^{-20} m^2.

Sample Description

Two samples of Green River shale 145 mm in diameter by 150 mm and 165 mm in length were obtained from RE/SPEC Inc. Rapid City, South Dakota. The samples were dry, having been exposed to ambient conditions for an unknown period of time. One sample, designated GR/86/U24-0/1 was obtained from a vertical drill hole so that bedding is perpendicular to the core axis. The second sample, GR/86/H212-0/1 was obtained from a horizontal drill hole.

In a hand specimen, the Green River Shale can be described as a dolomitic marlstone with a finely laminated yellowish-grey and brown mixture of organic and inorganic material. Detailed mineralogic description (Lee 1987) is found in

Test Apparatus

Measurement of fluid permeabilities in the micro-and nanodary (10^{-18} m^2 to 10^{-21} m^2) range places extreme demands on test system performance because of the long test durations and minute quantities of fluid flowing through the sample. The key measurement in these tests is the decay over

time of the differential pressure across the sample. Fluctuations in these measurements due to leaks and environmental temperature changes must be small in comparison to pressure changes induced by the fluid moving through the sample. The system-related pressure fluctuations also place restrictions on the minimum value of the initial differential pressure pulse applied to the sample. The test apparatus was designed to minimize these fluctuations while maintaining conditions such that the theoretical solution for the limiting case of small sample specific storage (equation 4) remained valid.

A schematic representation of the experimental apparatus is shown in Figure 2. Nitrogen gas confining pressure is provided by a 34.5 MPa maximum output compressor. Because of pressure surges accompanying the on-off operation of the compressor source produce similar surges in the pore pressure system, the compressor does not operate during a test. A large volume accumulator in line with the pressure vessel is used to compensate for small leaks and gas volume changes in response to temperature changes. Pressure inside the vessel is monitored by a Heise pressure gauge and a Dynisco pressure transducer.

The pore pressure system is conceptually similar to that used by Brace *et al.* [1968] though several modifications were required in order to perform measurements at elevated temperatures. The pore fluid system is comprised of an upstream and a downstream reservoir connected to the sample top and bottom as shown (Figure 2). The reservoirs are isolated from each other and the external pressure source, by closing valves A and B. To reduce spurious differential pressures generated by fluctuations in ambient temperature, the reservoirs are maintained in a controlled 50 ° C environment.

In order to approximate test conditions in which the specific storage of the sample is small in comparison to the compressive storage of the reservoir, the upstream reservoir volume is approximately 1.6×10^{-3} m^3. The downstream reservoir volume is 1.2×10^{-4} m^3, as small as possible to provide

measurable differential pressure changes.

If the unequal reservoir volumes were within the heated region inside the vessel, calculations show that temperature gradients and fluctuations on the order of 0.1 °C will induce a pore fluid pressure that will overwhelm differential pressure measurements. Three steps are taken to minimize potential adverse effects of temperature. First, the volume reservoirs are external to the test vessel. Second, the downstream reservoir is made large enough so that small thermal gradients along the length of the sample do not introduce spurious differential pressures; thus, the ratio of upstream to downstream reservoir volumes is 16:1. Third, care is taken to minimize pore fluid volumes on the upstream and downstream sides of the samples within the heated area (principally in the porous plates on the ends of the sample) and to assure that these volumes are in the same ratio as the reservoir the sample.

The upstream reservoir pressure is monitored by a Heise gauge and a Dynisco pressure transducer. Differential pressure between the upstream and the downstream reservoir is monitored by a Validyne differential pressure transducer. Pore pressure is generated using a dead weight tester hand pump.

The sample holding apparatus, Figure 3, contains the 37.9 mm long by 82.9 mm diameter sample. Porous plates, provided to ensure uniform distributions of fluid accorss the sample top and bottom, are located at the end of thee sample. As noted above, the pore volume ratio of these plates is approximately 16:1; the top plate (upstream reservoir side) is porous alundum while the lower plate is sintered stainless steel.

A double sheath arrangement encloses the sample-porous plate stock. The inner sheath is viton while the outer is copper. Between the two sheaths is silicone oil. The double sheath arrangement was necessary because, over the long test duration, the permeability of viton to nitrogen was not sufficiently low enough to prevent the buildup of gas pressure in the pore fluid system.

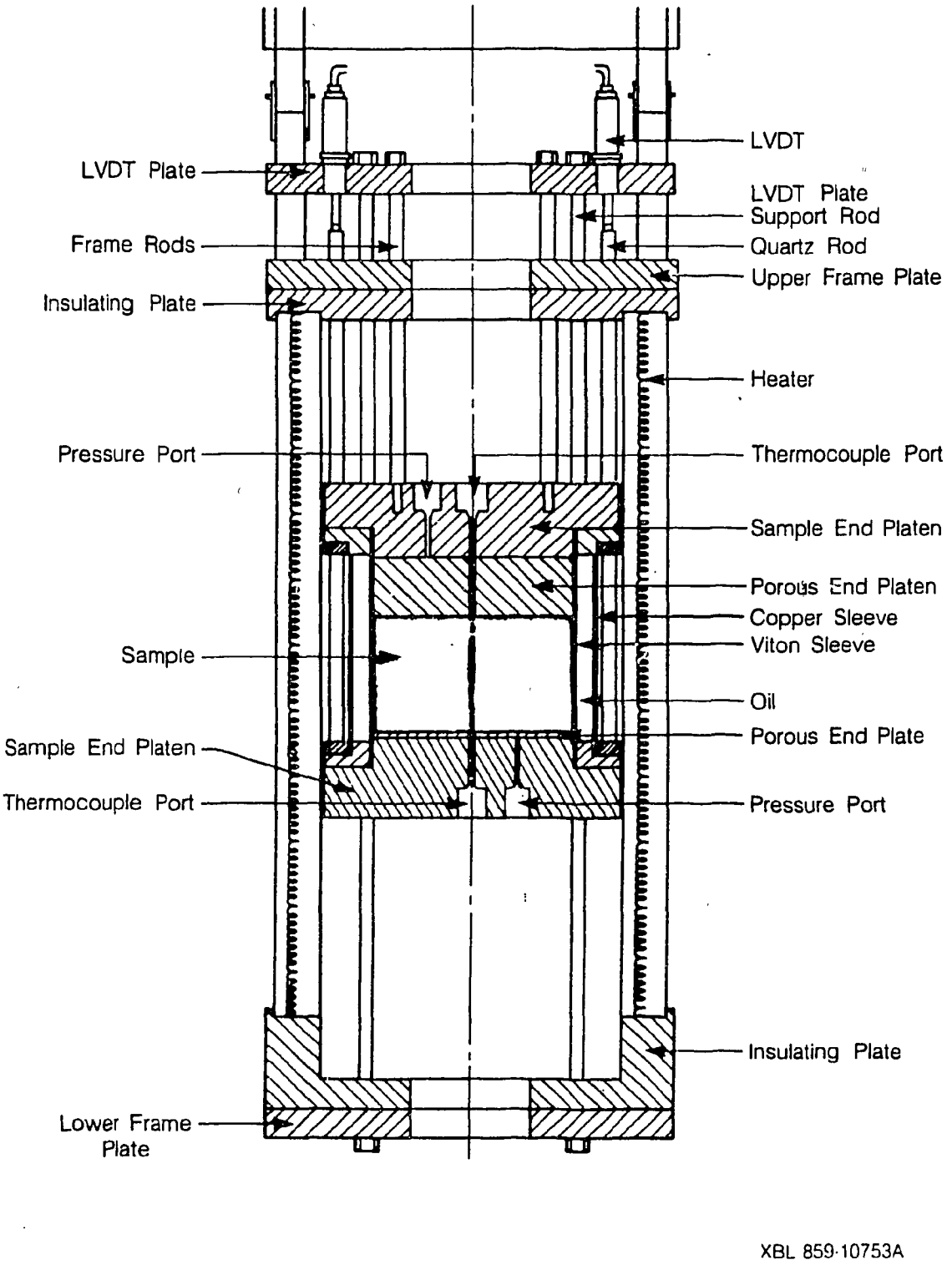

Figure 3. Detailed cross section of sample holding apparatus for permeability measurements.

As shown in Figure 3, the sample is located approximately at mid height of the 0.3 high heater, thus minimizing thermal gradients along the length of the sample. Type K thermocouples protrude through the sample endcaps to the top and bottom surfaces of the sample. An additional thermocouple is located at the centerline of the sample between the copper sheath and the heater elements. This the the temperature sensor for the RFL Model 76k1 temperature controller.

The capability of measuring sample deformation is provided by two precision LVDTs which sense motion in fused quartz rods attached to the sample endcap. Deformation measurements were not, however, made during permeability testing of the green River Formation samples.

Test Procedures

To perform a test the sample is first saturated with pore fluid using a vacuum saturation process. In this process the dry sample and porous plates are flooded with pore fluid after being in a desiccator jar under vacuum for approximately 24 hours. The sample and plates remain in the fluid under vacuum for approximately 3 hours. The desiccator jar is then opened to air pressure and the sample and porous plates remain in the fluid until they are placed in the sample holder. After placement of the sample in the pressure vessel, confining pressure is increased to approximately 3.5 MPa and a check for gas in the pore fluid lines exiting the vessel is made to assure that nitrogen is not leaking into the pore fluid system. Confining pressure is then increased slowly to the desire level. Simultaneously, pore presure is increased by the dead weight tester hand pump, keeping a 3.5 MPa differential between the pore fluid pressure and confining pressure, until the desired pore pressure is obtained.

Next, temperature is slowly increased at an approximate rate of 0.1 ° C/min to the desired level while maintaining constant confining and pore

pressure levels. Previous studies on granite (Richter and Simmons 1974) suggest that a heating rate of less than 2 °C/min should be used to minimize microstructural damage (cracking) due to thermal gradients.

The system is allowed to equilibrate under constant temperature and pressure conditions for at least 24 hours. A pressure pulse is then introduced into the pore fluid system. Normally the pulse (either an increase or decrease in pressure) is applied to the larger volume upstream reservoir. For low porosity samples, such as those from the Green River Formation, the pressure pulse can be applied to either reservoir. Results described in the next section were obtained from lowering the pressure in the downstream reservoir.

Results and Discussion

System Response Tests

As noted above it was important to minimize system-related fluctuations in differential pressure measurements. Having designed the test apparatus to minimize the fluctuations, system response tests were still required to check system performance. Results of these tests and implications of these results on the selection of the differential pulse magnitude are discussed below.

System performance was evaluated by performing tests in which an aluminum slug was substituted for the rock sample. Under ideal conditions with an impermeable sample, differential pressure across the sample should remain constant. This, however, was not observed. Results of a test exhibiting typical system response are shown in Figure 4. For this test the system was brought to equilibrium with a pore fluid pressure of 8.7 MPa at a temperature of 138 °C. A differential pressure of about 5.3 MPa was then imposed on the aluminum sample by lowering the pressure in the downstream reservoir. Time of zero in Figure 4 corresponds to the application of the pressure pulse. As shown in the figure, an initial sudden decrease in differential pressure was followed by a slow increase over about 30 hours. After 30 hours

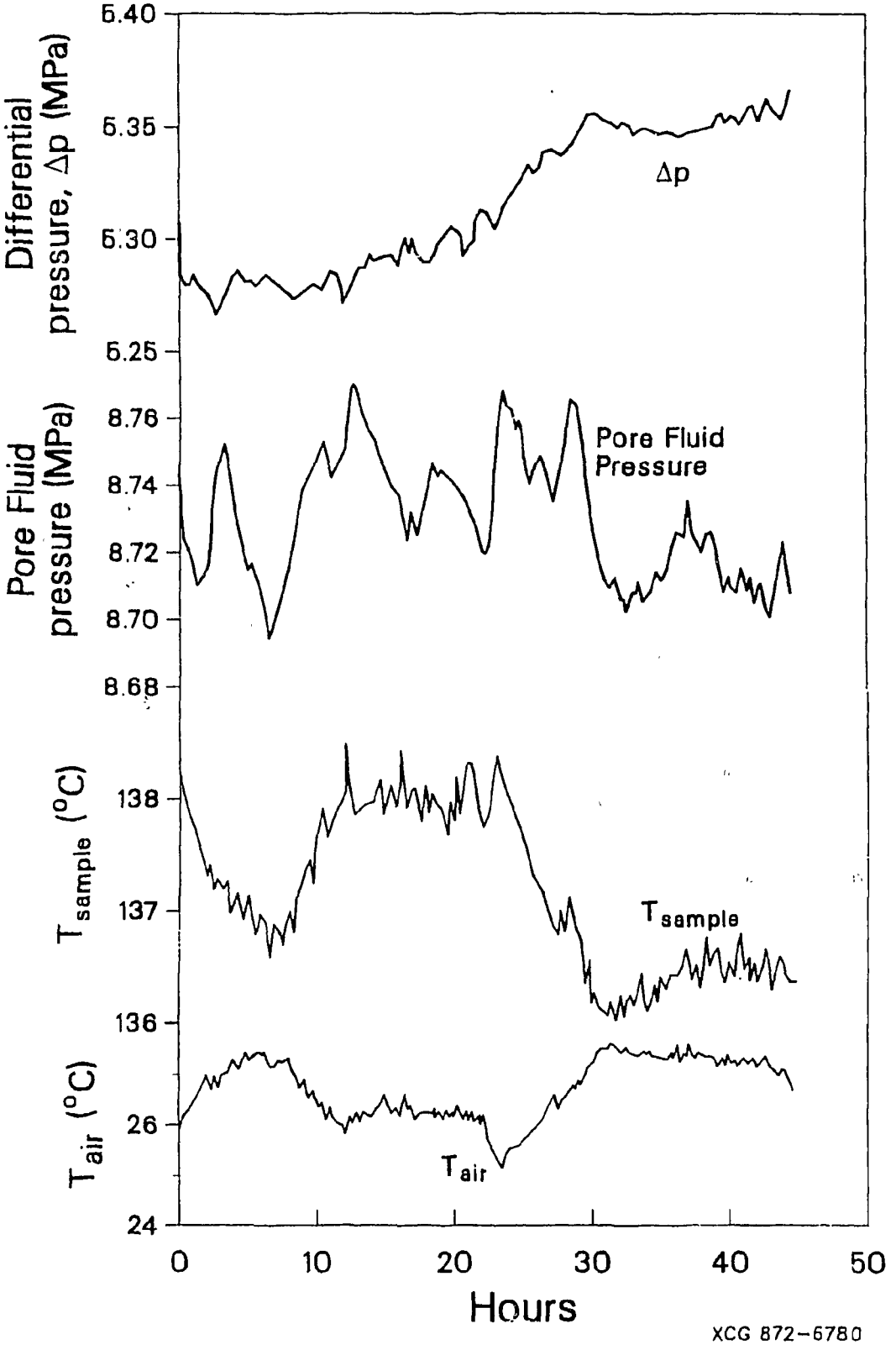

Figure 4. Results of system calibration test with aluminum sample at 138° C and 8.8 MPa pore fluid pressure.

the differential pressure approached a stable value. Additional variations reflect the drift in sample temperature.

Other tests performed at ambient temperature with pore fluid pressures of 9.6 MPa and 3.4 MPa and differential pressures of 0.7 MPa and 0.03 MPa, respectively, also exhibited the same general trend, though the magnitude of differential pressure change and the time to approach a stable value differed. For the test at 0.03 MPa differential pressure and 3.4 MPa pore fluid pressure, the differential pressure approached a stable value after about two hours with a concomitant 0.03 MPa increase in differential pressure. At 9.6 MPa pore fluid pressure and 0.7 MPa differential pressure a stabilized differential pressure was approached after 20 hours with an accompanying 0.1 MPa increase in differential pressure. In both tests, after the stabilized value had been obtained, additional variations in differential pressure amounted to less than 0.01 MPa. Though the general trends in differential pressure response for the aluminum tests were the same under different temperature/pressure conditions, there was enough variability in detail to preclude development of calibration factors for correction of shale measurements.

In addition to illustrating the differential pressure changes, results of the system response test shown in Figure 4 also show the pore pressure and temperature stability of the test system. As can be seen, both the air and the sample temperature (measured at the sample top) varied by about 3 ° C over thee course of the experiment, with the drift in sample temperature being a mirror image of the air temperature trends. This behavior resulted from temperature dependent electronics in the temperature controller. The pore pressure, measured in the upstream reservoir, exhibited cyclic variations with a maximum value of about 8.8 MPa and a minimum value of about 8.7 MPa. The general trend appears to follow the drift in sample temperature. It is important to note that variations in pore pressures of up to 0.1 MPa did not result in more than about a 0.01 MPa variation in the differential pressure trend.

The magnitude of the differential pressure change in the aluminum tests indicates the uncertainty introduced into the shale measurements by system response. For the initial one to five hours after application of the differential pressure pulse, results indicate that system response introduces an uncertainty of 0.03 MPa to 0.1 MPa. After a test has been in progress for 20 hours, however, the uncertainty due to system response diminishes to less than 0.01 MPa.

In order to measure permeabilities in the sub-nanodary range at the pore pressures of interest in this investigation, it was clear from the aluminum tests that a differential pressure pulse in excess of 10% of the pore pressure was required. For a differential pulse of 1.1 MPa (10% of 11 MPa) the differential pressure change across a sample of 10^{-23} m^2 permeability would be less than 0.03 MPa in a 100 hour test. Such small pressure changes would be obscured by the system response. Therefore, for the Green River Formation tests, pressure pulse magnitudes in the range of 6.2 MPa to 6.9 MPa were used.

Green River Formation Measurements.

Hydraulic conductivity measurements were performed on two samples with the bedding oriented parallel to the direction of flow. All tests were performed under the same confining pressure and pore pressure conditions of approximately 20.7 MPa and 11 MPa, respectively. One sample was tested at three temperature states: ambient, 72 ° C, and 131 ° C. The second sample was tested at 140 ° C. Test conditions for each measurement are tabulated in Table I and Appendix B. Note that pore pressure measurements represent the fluid pressure conditions in the upstream reservoir.

Figure 5 shows the test conditions for the second sample. Time equal to zero corresponds to the application of the differential pressure pulse. The decrease in differential pressure reflects the movement of water through the sample from the upstream reservoir to the downstream reservoir.

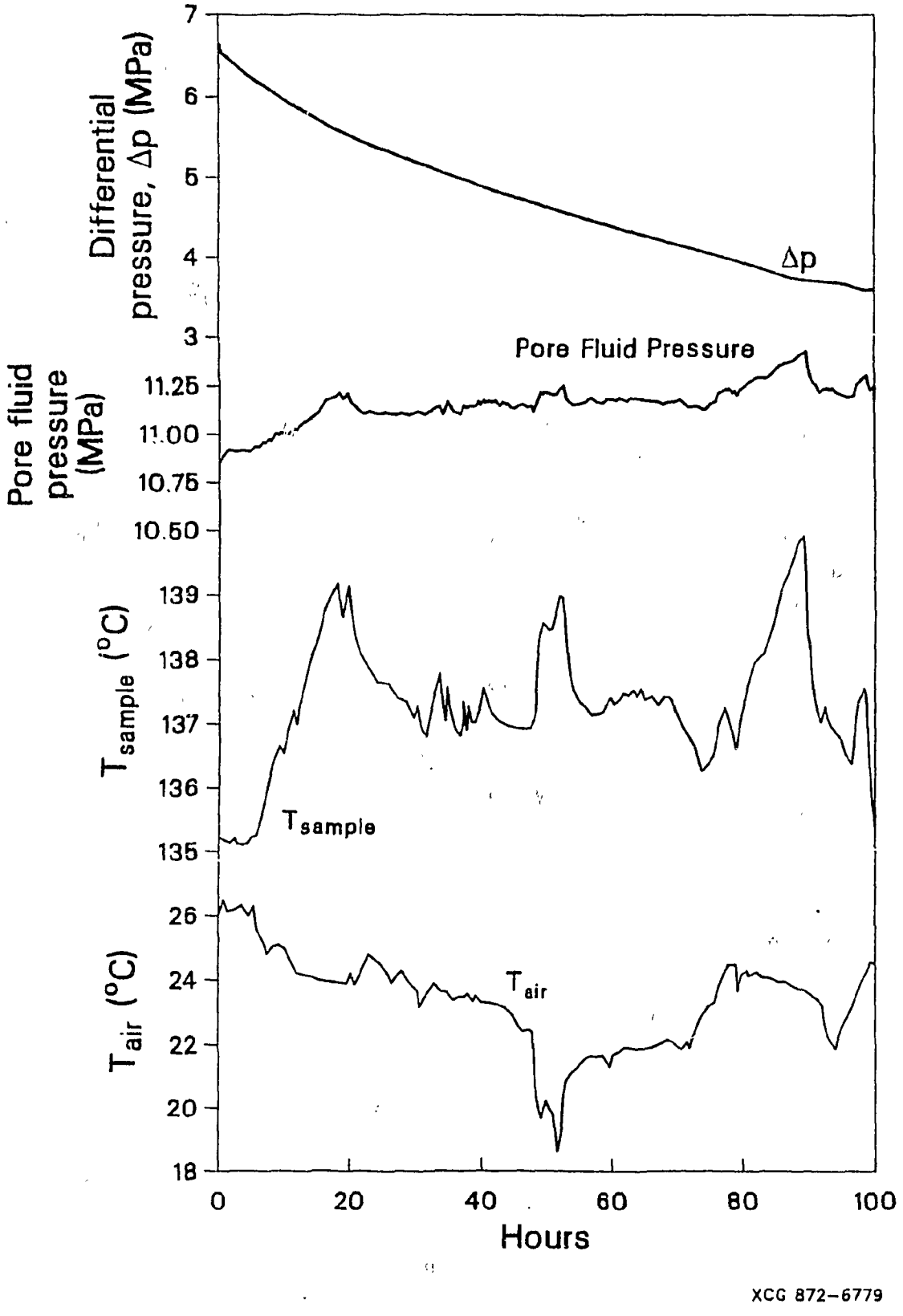

Figure 5. Results of Green River shale test at 140° C and confining and pore pressures of 20.7 MPa and 11 MPa, respectively, (T_{sample} measured at sample bottom).

Also shown in Figure 5 are the variations in pore pressure measured in the upstream reservoir and in the sample temperature. Sample temperature variations were cyclic in nature with the difference between the minimum and maximum of about 5.0 ° C. The pore pressure variations were also cyclic, with the maxima corresponding to the minima in sample temperature. The variations in temperature and pore pressure were not reflected in the differential pressure measurements. This means that the downstream reservoir pressure exhibited the same pressure fluctuations as the upstream reservoir and therefore did not affect the pressure gradient across the sample. Based on these observations and the aluminum sample tests, it was concluded that the pore pressure and sample temperature fluctuations had negligible effect on the hydraulic conductivity measurements.

The differential pressure data from all tests are presented in Figure 6, which is a plot of the logarithm of the ratio of the initial pressure pulse magnitude (PP) to differential pressure (ΔP) at time t. Hydraulic conductivity was determined by taking the slope of the least squares best fit straight line passed through these curves, and applying the fit to equation [4]. The correlation coefficients obtained from the regression analyses were greater than 0.95 for all tests. Upstream and downstream reservoir compressive storage was assumed to be equal to that of the water alone. Considering the thick-walled stainless steel construction of the volume reservoir, there is probably little error in this assumption. Reservoir compressive storage, however, will be measured at a later date. Using values of fluid viscosity calculated through an empirical equation deduced by Ozbeck *et al.* [1977], and specific gravity derived from an equation for density in the *CRC Handbook of Chemistry and Physics,* the measured hydraulic conductivities were converted to absolute permeabilities. Results are tabulated in Table 1 and in Appendix B.

Table 1. Green River shale test summary

Test No	Temp °C	P_p (MPa)	P_c (MPa)	PP (MPa)	Hyd. Cond (m/s)	Permeabililty (m^2)
1	24	10	20.7	6.4	1.61×10^{-16}	1.5×10^{-23}
2	74	11.2	20.7	6.2	4.83×10^{-16}	2×10^{-23}
3	130	10.5	21	6.9	4.23×10^{-15}	1×10^{-22}
4	137	11.1	21	6.6	5.96×10^{-15}	1.5×10^{-22}

Results presented in Table I show that the permeability of Green River Formation, though very low, increases by about an order of magnitude over the temperature range of room to 140 ° C. Results also show that this increase is nonlinear with temperature; the increase being greater at high temperatures than at low temperatures. These trends are consistent with the changes in mechanical properties with temperature observed in many rocks. Nonlinear decreases in moduli and increases in thermal expansion with increasing temperature have been observed by Richter and Simmons [1974], Heard and Page [1982], Myer [1985], and many others. It is believed that these changes in mechanical properties are related to microcrack growth and increase in microcrack density as a result of heating. A plausible explanation for the observed increase in permeability with temperature is that heating resulted in an increase in interconnected microcrack porosity. If porosity has increased due to additional microcracking, the permeability measurements should exhibit hysteresis upon temperature cycling. Repeat tests at room temperature conditions of a sample previously heated will be performed to investigate this behavior.

Results presented in Figure 6 exhibit some nonlinearity at times between zero and 5 to 10 hours. This nonlinearity may reflect the characteristic system response as described in the previous section or the nonzero specific storage of the sample. Data from the first 5 hours were not included in the

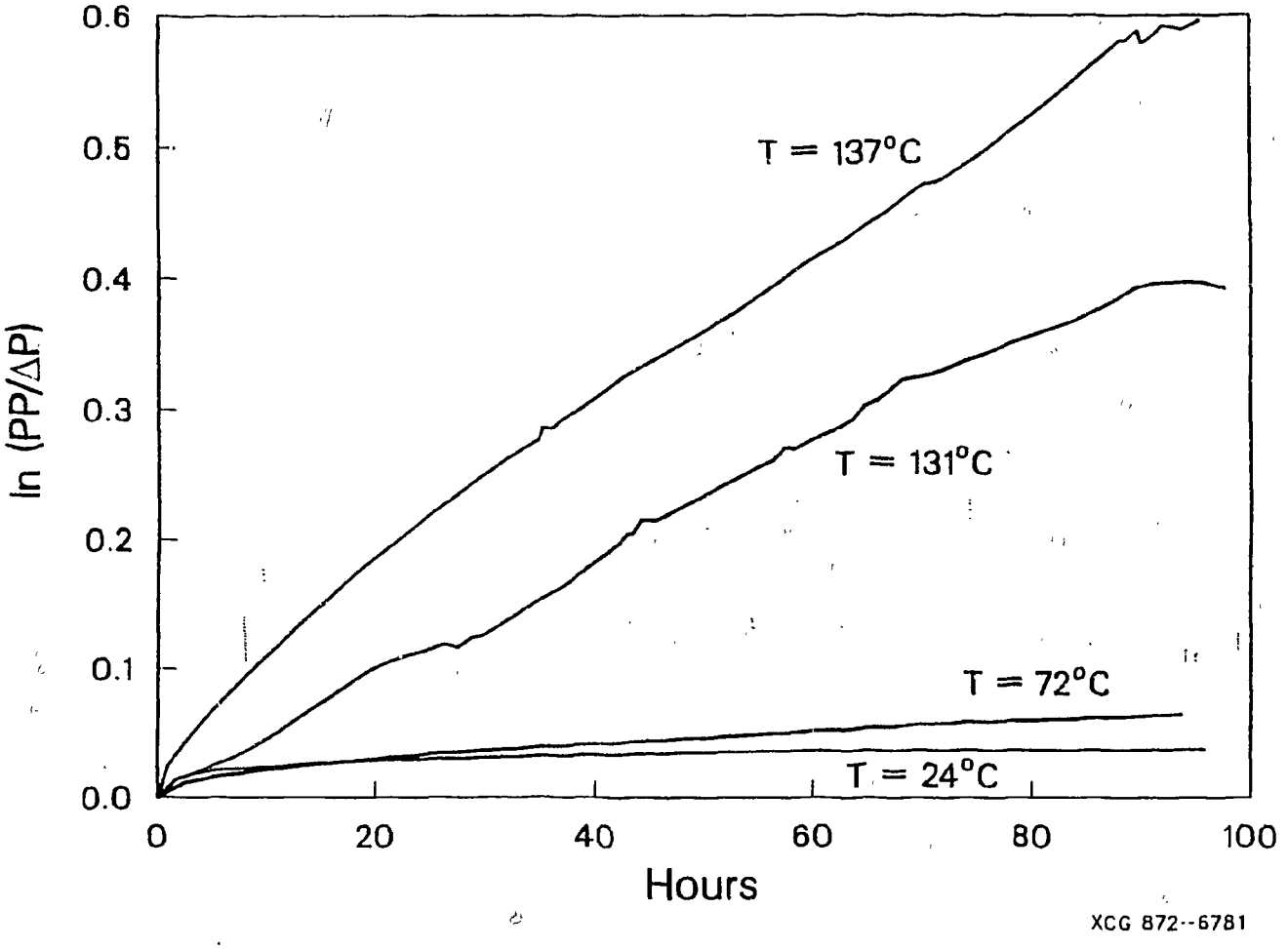

Figure 6. Effects of temperature on pressure pulse decay for four tests on Green River Formation. Pulse decay plotted as the logarithm of the ratio of the initial pressure pulse magnitude to the differential pressure reading.

least squares analyses.

Test 4 was conducted because it was felt the temperature instability experienced in test 3 may have affected the permeability measurements. It is believed that the temperature rise in test 3 caused the fluid pressure in the upstream and downstream reservoirs to increase, therefore changing the effective stress state in the sample. The differences between results of the two tests reflect the effect of the varying effective stress state in test 3. Additional tests are planned to investigate the influence of effective stress state on the permeability of shales. These additional tests will also provide data to evaluate the effects of the large pressure pulse used in these experiments.

Summary and Conclusions

A method of measuring the hydraulic conductivity of low permeability shale as a function of pressure and temperature has been developed and successfully demonstrated. Measurements have been performed on samples of Green River Formation up to a temperature of 140 ° C. For flow parallel to bedding hydraulic conductivities increased nonlinearly from 1.75×10^{-16} m/s (1.6×10^{-23} m^2) at 25 ° C, to 5.6×10^{-15} m/s (1.4×10^{-22} m^2) at 140 ° C. This increase in permeability with temperature may reflect an increase in microcrack porosity resulting from the heating. Further testing will be performed to investigate the effect of temperature on the permeability of Pierre Shale and a Devonian shale, each of which have very different mineralogies from the Green River Formation. Additional tests will also be performed to investigate effects of pressure pulse magnitude and effective stress state on shale permeability.

References

Bernabe, Y., 1986, The Effective Pressure Law for Permeability in Chelmsford Granite and Barre Granite: Int. J. of Rock Mech. Min. Sci. and Geomech. Abstr., v. 23, n. 3, pp. 267-275.

Bernabe, Y., 1987, The Effective Pressure Law for Permeability During Pore Pressure and Confining Pressure Cycling of Several Crystalline Rocks: J. of Geophys. Res., v. 92, N1 B1, pp. 649-657.

Brace, W.F., Walsh, J.B., and Frangos, W.T., 1968, Permeability of Granite Under High Pressure: J. Geophys. Res., v. 73, pp. 2225-2236.

Brace, W.F., 1980, Permeability of Crystalline and Argillaceous Rocks: Int. J. Rock Mech. Min. Sci. & Geomech. Abstr., v. 17, pp. 241-251.

Croff, A.G., Lomenick, T.F. Lowrie, R.S., and Stow, S.H. 1987, Evaluation of Five Sedimentary Rocks other than Salt for High Level Nuclear Waste Repository Siting Purposes, ORNL 6241, three volumes.

CRC Handbook of Chemistry and Physics, CRC Press Inc., 1985-1986, 66th Ed.

Heard, H.C., 1980, Thermal Expansion and Inferred Permeability of Climax Quartz Monzonite to 300 C and 27.6 MPa: Int. J. Rock Mech. Min. Sci & Geomech. Abst., v. 17, pp. 289-296.

Heard, H.C. and Page, L., 1982, Elastic Moduli, Thermal Expansion, and Inferred Permeability of Two Granites to 350°C and 55 Megapascals; J. of Geophy. Res., v. 86, B11, pp. 9340-9348.

Hsieh, P.A., Tracy, J.V., Neuzil, C.E., Bredehoeft, J.D., and Silliman, S.E., 1981, A Transient Laboratory Method for Determining the Hydraulic Properties of 'Tight' Rocks-I. Theory: Int. J. Rock Mech. Min. Sci. and Geomech. Abstr., v. 18, p. 245-252.

Jones, F.O. and Owens, W.W., 1980, A Laboratory Study of Low-Permeability Gas Sands: J. Pet. Tech., Sept. 1980, pp. 1631-1640.

Jones, F.O., 1975, A Laboratory Study of the Effects of Confining Pressure on Fracture Flow and Storage Capacity in Carbonate Rocks: Jour. of Pet. Tech., v. 27, pp. 21-27.

Kranz, R.L., Frankel, A.D., Engelder, T. and Scholz, C.H., 1979, The Permeability of Whole and Jointed Barre Granite: Int. J. of Rock Mech. and Min. Sci. Abstracts, v. 16, pp. 225-234.

Lee, S4, 1987 Personal communication, Oak Ridge National Laboratory

Mitchell, J.T., 1976, Fundamentals of Soil Behavior, John Wiley and Sons, Inc., New York, p. 346.

Myer, L.R., 1985, Electro-servo Control System for Thermomechanical Properties Testing: Geotech. Testing J., v. 8, no. 4, pp. 171-178.

Neuzil, C.E., Cooley, C., Silliman, S.E., Bredehoeft, J.D., and Hsieh, P.A., 1981, A Transient Laboratory Method for Determining the Hydraulic Properties of 'Tight' Rocks-I. Theory: Int. J. Rock Mech. Min. Sci. and Geomech. Abstr., v. 18, pp.. 245-252.

Ozbek, H., Fair, J.A. and Phillips, S.L., 1977, Viscosity of Aqueous Sodium Chloride Solutions from 0-150 ° C: Energy and Environment Division, LBL., U.C. Berkeley, LBL-5931.

Richter, D. and Simmons, G, 1974, Thermal Expansion Behavior of Igneous Rocks: Int. J. Rock Mech. Min Sci. and Geomech. Abstract, v. 11, pp. 403-411.

Rida, D.C. and Hadley, G.R., 1986, Saturated Permeability Measurements on Pumice and Welded-Tuffaceous Materials: Environ. Geol. Water Sci., v. 8, pp. 137-145.

Summers, R., Winkler, K. and Byerlee, J., 1978, Permeability Changes During the Flow of Water Through Westerly Granite at Temperatures of 100 ° C-400 ° C.: J. of Geophys. Res., v. 83, B1, pp. 339-344.

Trimmer, D., Bonner, B., Heard, H.C. and Duba, A., 1980, Effect of Pressure and Stress on Water Transport in Intact and Fractured Gabbro and Granite: J. of Geophys. Res., v. 85, B12, pp. 7059-7071.

Waldur, J. and Nur, A., 1986, Permeability Measurement by the Pulse-Decay Method: Effects of Poroelastic Phenomena and Non-Linear Pore Pressure Diffusion: Int. J. Rock Mech. Min. Sci. and Geomech. Abstr., v. 23, pp. 225-232.

Walsh, J.B. and Brace, W.F., 1984, The Effect of Pressure on Porosity and the Transport Properties of Rock: J. Geophysical Res., v. 89, no. B11, pp. 9425-9431.

Young, A., Law, P.F., and McLatchie, A.S., 1964, Permeability studies of Argillaceous Rocks. J. Geophys. Res., V. 69 No. 20. pp. 4237-4245.

Zoback, M.D., and Byerlee, J.D., 1975, The Effect of Mircocrack Dilatancy on the Permeability of Westerly Granite: J. Geophy. Res., v. 80, p. 752-755.

Appendix A

A representative sample of the Green River Formation was chemically digested and fractionated according to grain size, then characterized mineralogically via x-ray diffractometry (XRD). The results are as follows:

Major Mineral Importance in bulk Sample:

dolomite>quartz>feldspar>calcite

Grain size and Relative Importance of Major Minerals:

Grain Size	Weight%	Relative Importance of Mag minerals
180-53 mm	0.02	NA
53-2 mm	54.40	dol>qtz
2-0.2 mm	13.06	qtz>dol
<0.2 mm	31.92	qtz>ill

Oxidation Composition:

Compound	Wt%	Element	PPM
SiO_2	34.24	Fe	21000
CO_3	26.4	Sr	630
CaO	13.16	Ba	500
Al_2O_3	7.56	Mn	400
MgO	6.35	P	320
Na_2O	0.7	Cr	83
		V	77
total S	0.34	Ni	<55
Sulfide S	0.3	Mo	<36
T_iO_2	0.27	Cu	20
SO_4	0.12	Zn	<18
	89.44	Co	9.7

Appendix B

System Parameters and Test Results

Green River Shale Test #1

System Parameters

	Avg	Min	Max	Difference	Comments
P_p (MPa)	10.17	9.58	10.42	0.84	Unreliable; temperature sensitive electronics
P_c (MPa)	20.65	20.48	20.8	0.32	Unreliable; temperature sensitive electronics
T_{sam} (C)	4.6	22.9	25.7	2.8	
T_{air} (C)	24.6	22.9	25.7	2.8	

P_p = pore pressure
P_c = confining pressure
T_{sam} = sample temperature

Pulse magnitude	=	6.56 MPa
decayed to:		6.32 MPa
decrease of:		0.24 MPa
Permeability	=	1.6×10^{-23} m^2
Hydraulic conductivity	=	1.75×10^{-6} m/s

Evaluation Parameters

slope	=	4.999×10^{-8} /s
correlation coeff	=	0.953716
sample diameter	=	$8.29\ 10^{-2}$ m
sample length	=	3.81×10^{-2} m
fluid viscosity	=	8.956×10^{-4} Ns/m^2
fluid specific weight	=	9777.9 N/m^3
upper res. comp. storage	=	7.12×10^{-9} m^2
lower res. comp. storage	=	5.35×10^{-10} m^2

Green River Shale Test #2
System Parameters

	Avg	Min	Max	Difference	Comments
P_p (MPa)	11.11	10.74	11.78	1.04	
P_c (MPa)	20.58	20.43	20.73	0.30	Unreliable; temperature sensitive electronics
T_{sam} (C)	74.65	70.11	81	10.89	
T_s (C)	74.34	69.94	80.89	10.75	
T_{air} (C)	25.04	23.33	27	3.67	

P_p = pore pressure
P_c = confining pressure
T_{sam} = temperature of sample
T_s = temperature at sample midheight

Pulse magnitude = 6.25 MPa
decayed to: 5.85 MPa
decrease of: 0.40 MPa

Permeability = 2.15×10^{-23} m^2
Hydraulic conductivity = 5.38×10^{-16} m/s

Evaluation Parameters

slope = 1.53×10^{-7} /s
correlation coeff = 0.989963
sample diameter = 8.29×10^{-2} m
sample length = 3.81×10^{-2} m
fluid viscosity = 3.88×10^{-4} Ns/m^2
fluid specific weight = 9606.2 N/m^3
upper res. comp. storage = 7.124×10^{-9} m^2
lower res. comp. storage = 5.35×10^{-10} m^2

Green River Shale Test #3
System Parameters

	Avg	Min	Max	Difference	Comments
P_p (MPa)	10.48	9.43	12.02	2.59	
P_c (MPa)	21.03	20.63	21.42	0.79	Unreliable; temperature sensitive electronics
T_{sam} (C)	121.6	115	146.6	31.6	
T_s(C)	130.7	114.4	145.7	31.3	
T_{air} (C)	25.5	22	28.4	6.4	

P_p = pore pressure
P_c = confining pressure
T_{sam} = temperature of sample
T_s = temperature at sample midheight

Pulse magnitude = 6.9 MPa
decayed to: 4.65 MPa
decrease of: 2.27 MPa

Permeability = 1.09×10^{-22} m^2
Hydraulic conductivity = 4.36×10^{-15} m/s

Evaluation Parameters

slope = 1.244×10^{-6} /s
correlation coeff = .998203
sample diameter = 8.29×10^{-2} m
sample length = 3.81×10^{-2} m
fluid viscosity = 2.34×10^{-4} Ns/m^3
fluid specific weight = 9200.3 N/m^2
upper res. comp. storage = 7.12×10^{-9} m^2
lower res. comp. storage = 5.35×10^{-10} m^2

ORNL/Sub/85-21674/1
Dist. Categories UC-11,-70

INTERNAL DISTRIBUTION

1. A. G. Croff
2. C. S. Haase
3. R. D. Hatcher
4. D. D. Huff
5. G. K. Jacobs
6. R. Ketelle
7. D. W. Lee
8. S. Y. Lee
9. T. F. Lomenick
10. G. K. Moore
11. J. Nyquist
12. T. H. Row
13. D. K. Solomon
14-23. S. H. Stow
24. L. Toran
25. V. S. Tripathi
26. K. L. Von Damm
27. R. G. Wymer
28. G. T. Yeh
29-30. Central Research Library
31. ORNL Patent Section
32-33. Laboratory Records
34. Laboratory Records, ORNL RC
35. ORNL-Y-12 Technical Library Document Reference Section

EXTERNAL DISTRIBUTION

DOE-ORO, P. O. Box E, Oak Ridge, TN 37831

36. Office of Assistant Manager for Energy Research and Development

DOE-Office of Civilian Radioactive Waste Management, Washington, DC 20545

37. A. J. Jelacic
38. S. H. Kale
39. R. Stein

Office of Waste Technology Development, Battelle Project Management Division, 7000 S. Adams Street, Willowbrook, IL 60521

40-41. W. E. Newcomb
42. G. L. Stirwalt
43. A. K. Yonk

DOE-CHO, 9800 S. Cass Ave., Chicago, IL 60439

44. R. C. Baker
45. J. D. Kasprowicz
46. S. Mann

Department of Petroleum Engineering and Geophysics, Texas A&M University, College Station, TX 77843

47. P. A. Domenico

RE/SPEC Inc., P. O. Box 725, Rapid City, SD 57701

48. A. Fossom
49. P. Gnirk
50. J. Ratigan

Berkeley Hydrotechnique, 2030 Addison St., Suite 500, Berkeley, CA 94704

51-55. B. Y. Kanehiro

Lawrence Berkeley Laboratory, Berkeley, CA 94720

56. T. Buscheck
57-66. L. Myer

U.S. Geological Survey, Federal Center Bldg. 25, Denver, CO 80225

67. M. Grout
68. E. R. Verbeek

69. Dr. D. G. Brookins, 3410 Groman Ct., N.E., Albuquerque, NM 87110

70. Dr. Serge Gonzales, Earth Resource Associates, Inc., 295 E. Doughterty Street, Suite 105, Athens, GA 30601

71. Dr. K. S. Johnson, Earth Resource Associates, 1321 Greenbriar Drive, Norman, OK 73069

72. Harry Smedes, 1126 Buehler Drive, Las Vegas, NV 89102

73-401. Given distribution as shown in TIC-4500 under UC-11, Environmental Control Technology and Earth Sciences, and UC-70, Nuclear Waste Management categories.